

SHELL FLASHES ON ACCRETING NEUTRON STARS AND X-RAY BURSTS

MASAYUKI Y. FUJIMOTO^{1,2}

Department of Astronomy, University of Illinois

AND

TOMOYUKI HANAWA AND SHIGEKI MIYAJI

Department of Astronomy, University of Tokyo

Received 1980 March 5; accepted 1980 December 18

ABSTRACT

When gas is accreted onto a neutron star, nuclear burning is rekindled on the surface. The thermal stability of shell burning and the progress of shell flashes are studied using the semianalytical method to explain the mechanism that causes variations in the burst profile of type I X-ray bursts. Hydrogen-shell burning is found to be stabilized for a relatively high accretion rate because of the saturation of CNO cycles set by intervening β -decays, while helium-shell burning is thermally unstable. Therefore, shell flashes are triggered in three different ways, depending on the accretion rate: (1) the combined helium and hydrogen shell flash ignited in the stable hydrogen-burning shell for the highest range of accretion rate; (2) the pure helium-shell flash below the steady state hydrogen-burning shell for the intermediate range; and (3) the hydrogen-shell flash developing into the combined helium and hydrogen shell flash for the lowest range. The progress of nuclear reactions during these shell flashes is followed numerically, showing that the shell flashes grow in various strengths depending on the mixture of helium and hydrogen as well as on the pressure of the burning shell. Based on these results, it is proposed that two different modes of type I X-ray bursts are reproduced by the two cases of lower accretion rate, while the case of the highest accretion rate is observed as bright bulge sources where shell flashes are obscured by the optically thick accreting flow.

Subject headings: nuclear reactions — stars: accretion — stars: neutron — X-rays: bursts

I. INTRODUCTION

Type I X-ray bursts were discovered in 1975 and have recently revealed a variety of burst profiles. According to observations by the *Hakucho* satellite, they are classified into two typical groups, fast and slow modes. The fast mode contains the popular type I X-ray bursts which have rapid rise times ($\lesssim 1$ s) and are of short duration (\approx several seconds). The slow mode was newly classified by Murakami *et al.* (1980a) and is characterized by relatively slow rise times (\approx several seconds) and by long duration (up to a few dozen seconds). (Typical time scales are taken, for example, from the observation of transient X-ray source 1608-522.) Transitions from the fast to slow mode was observed during the recurrences of bursts, and some correlations were observed between the burst modes and the persistent X-ray luminosity (Murakami *et al.* 1980a). Theoretical models should account for these new observations.

It has been suggested that type I X-ray bursts originate from nuclear shell flashes caused by the accretion of matter onto the surface of a neutron star (Woosley and Taam 1976; Maraschi and Cavaliere 1978). Joss (1978) computed models of helium-shell flashes on an accreting

neutron star to compare with observations. In spite of his success in reproducing some properties of the fast mode, these models have involved the following problems. As Joss neglected the hydrogen-rich layer, the structure of the envelope is determined only by the heat flow from the inner core, i.e., by the core temperature T_c of a neutron star. When T_c is specified, the mass of the accreted envelope before the ignition of the helium-shell flash is determined uniquely by T_c and independently of the accretion rate. Therefore, shell flashes recur under the same conditions, making it difficult to explain the variations in burst profile. Moreover, we see below that the assumed values of T_c are too high to be realized during the actual evolution.

The thermal structure of the accreted envelope on a neutron star has been investigated using the steady state approximation by Hansen and Van Horn (1975) and by Taam and Picklum (1978). In the latter models, the base of the hydrogen-burning shell is found to lie at such a high density that it overlaps with the helium-burning shell because of the very thin envelope and because of the saturation of the hydrogen-burning rate set by β -decays in CNO cycles. Incorporating the presence of the hydrogen-rich material, Taam and Picklum (1979) computed the evolution of shell burnings and demonstrated that the hydrogen-shell flash leads to the ignition of helium burning. Their results also showed that the broadening of the burst profile is due to β -decays of unstable, proton-rich nuclei. These works suggest that

¹ On leave from Takada Branch, Niigata University, Joetsu-shi, Niigata, Japan.

² Supported in part by National Science Foundation grant AST 78-20124.

hydrogen-shell burning has crucial effects on the progress of shell burnings in an accreting neutron star.

In this paper, we study thermal properties of shell burnings and the progress of shell flashes in an accreting neutron star. Our purpose is to show the evolutionary paths through the helium-shell flashes and to reveal that hydrogen-shell burning plays important roles in the interpretation of the different modes of burst profiles.

Sugimoto and Fujimoto (1978) have advanced a general theory of shell burnings and have shown that they can be treated semianalytically. The analysis of accreting white dwarfs gives good agreement with numerical computations (see e.g., Sugimoto *et al.* 1979). We apply the same method to neutron stars since the semianalytical treatments are well suited for discussing the physics involved in shell burnings and for making their progress clear in a wide range of parameters.

In § II, we analyze the thermal stability of hydrogen and helium shell burnings. It is shown that there are three different ways to ignite helium-shell flashes, depending on the accretion rate. The progress of helium-shell flashes is investigated in § III in relation to the various situations characterized by hydrogen-shell burning. Shell flashes are shown to result in the various strengths relevant to the fast and slow modes of bursts. Conclusions and discussions are presented in § IV, together with correspondences between our results and observations by the *Hakucho* satellite.

II. THERMAL NATURES OF SHELL BURNINGS

a) Assumptions and Methods of Computations

The structure of the envelope in a neutron star is fairly simple. According to Sugimoto and Fujimoto (1978), the configuration of the shell in the envelope depends on the ratio V of its radial distance r from the center of the star to the pressure scale height H_p , i.e.,

$$V \equiv \frac{r}{H_p} = -\frac{d \ln P}{d \ln r} = \frac{GM_r \rho}{rP(1 - 2GM_r/rc^2)}. \quad (1)$$

Here and in the following, the usual notations for the theory of stellar structure (see e.g., Hayashi, Hōshi, and Sugimoto 1962) are used except when otherwise stated. Because of the large gravitational potential, the value of V is very large in the envelope of a neutron star. Even at the peak of shell flash, it remains as large as $V \sim 10^3$. This implies that such shells are flat in configuration so that the pressure P is determined only by the weight of the overlying layers without regard to the thermal state of the envelope (Hara, Ikeuchi, and Sugimoto 1976).

Thus, P at the bottom of the shell is related to the proper mass ΔM accumulated above it as

$$P = \frac{\Delta M(1 - 2GM/Rc^2)^{1/2}}{4\pi R^2} \frac{GM}{R^2(1 - 2GM/Rc^2)}, \quad (2)$$

where M and R are the mass and the radius of a neutron star. When M and R are specified, thermodynamical quantities of the shell are determined by ΔM and one more parameter, such as the temperature T or the specific

entropy s at the bottom of the shell. Given these two parameters at the bottom of the burning shell, the characteristics of nuclear shell burnings can be computed by using the thin-shell approximation (Hayashi, Hōshi, and Sugimoto 1962). The nuclear energy generation rate L_N in the envelope is given as

$$L_N = \left(1 + \frac{1}{n+1}v + \frac{1}{N+1}\eta - \frac{4}{V}\right)_b^{-1} \times \epsilon_{N,b} \Delta M \left(1 - \frac{2GM}{Rc^2}\right)^{1/2}, \quad (3)$$

where the energy generation rate per unit mass ϵ_N is approximated to be proportional to $\rho^n T^v$. Here and in the following, the subscript b denotes the bottom of the burning shell. Here, n and N are polytropic indices defined as

$$\begin{aligned} \frac{1}{n+1} &\equiv \frac{d \ln T/d \ln r}{d \ln P/d \ln r} \\ &= \min \left[\left(\frac{\partial \ln T}{\partial \ln P} \right)_{\text{ad}}, \frac{3\kappa P L_N}{16\pi a c T^4 G M} \left(1 - \frac{2GM}{Rc^2}\right) \right], \\ \frac{N}{N+1} &\equiv \frac{d \ln \rho/d \ln r}{d \ln P/d \ln r} \\ &= \left(\frac{\partial \ln \rho}{\partial \ln P} \right)_T + \left(\frac{\partial \ln \rho}{\partial \ln T} \right)_P \frac{1}{n+1}. \end{aligned} \quad (4)$$

The thermal condition in the shell is governed by the equation of energy conservation. It is convenient to use the mass fraction $q \equiv M_r/M$ as an independent variable, instead of the Lagrangian coordinate M_r , since the structure depends on $\Delta M = M(1 - q)$, as seen in equation (2). Then, the change in the specific entropy $s(q, t)$ at the bottom of the shell is expressed as

$$T \left(\frac{\partial s}{\partial t} \right)_q = \epsilon_N - \epsilon_v - \frac{\partial}{\partial q} \left(\frac{Lr}{M} \right) + \frac{\dot{M}}{M} T \frac{\partial s}{\partial \ln q}, \quad (5)$$

where ϵ_v denotes the energy loss rate per unit mass by neutrino processes, and where \dot{M} is the mass accretion rate $\dot{M} \equiv dM/dt$.

The most remarkable feature of a neutron star is that the time scale of heat diffusion in the envelope is very short, mainly because of the very small scale height. As compared to this heat diffusion, we can neglect the neutrino energy loss at the relevant densities and temperatures. The last term in the right-hand side represents the homologous term of so-called gravitational energy release $\epsilon_q^{(h)}$, i.e., the addition of entropy by the inward propagation of matter due to compression by accretion (Sugimoto and Nomoto 1975). As the gravitational potential is very large, the infalling matter liberates the energy more than 100 MeV per nucleon on the surface of the neutron star. The effect of $\epsilon_q^{(h)}$, however, is not so large because of the very small pressure scale height. The gravitational energy release in the envelope is evaluated in order of magnitude as $m_H(GM/R^2)H_p \approx 0.2-0.02$ MeV per nucleon (m_H is the atomic mass unit). This value is much smaller than the nuclear energy release of 7 MeV

per nucleon, and we can neglect this term when nuclear burning is active in the envelope.

The condition for the envelope in thermal equilibrium, $(\partial s/\partial t)_q = 0$, is then reduced to

$$\epsilon_N - \frac{\partial}{\partial q} \left(\frac{Lr}{M} \right) = 0. \quad (6)$$

In solving this equation, the derivatives are simply approximated with the divisions using the pressure scale height as

$$\frac{\partial}{\partial q} \left(\frac{Lr}{M} \right) \approx \epsilon_r \equiv \frac{4ac}{3} \frac{T^4}{\kappa \rho^2 H_p^2}. \quad (7)$$

In order to keep this thermal equilibrium configuration stationary, nuclear fuel must be supplied by the accretion as fast as it is consumed by nuclear burning. Under the steady state, the accretion rate \dot{M}_{st} is equal to the rate of consumption of nuclear fuel in the envelope which is related to the integral of nuclear energy generation rate L_N as

$$\dot{M}_{st} = L_N / X_N E_N, \quad (8)$$

where E_N (E_H or E_{He}) and X_N denote the nuclear energy release from a unit mass of nuclear fuel (hydrogen or helium) and its concentration in the envelope, respectively.

The stability of thermal equilibrium configurations can be studied by introducing perturbations into equation (5). Because the pressure remains constant throughout the shell flash, as seen in equation (2), the perturbation equation is expressed rather simply as

$$\frac{\partial \delta \ln T}{\partial t} = F \delta \ln T,$$

$$F \equiv \frac{\epsilon_r}{c_p T} \left[\frac{\epsilon_N}{\epsilon_r} v - 4 + \kappa_T + \left(\frac{\partial \ln \rho}{\partial \ln T} \right)_p \left(\frac{\epsilon_N}{\epsilon_r} \eta + \kappa_\rho \right) \right], \quad (9)$$

where κ_T and κ_ρ denote the temperature and the density dependences of opacity, respectively. When F is positive, the nuclear shell burning in a thermal equilibrium is unstable and makes a thermal runaway.

When the nuclear burning is extinct, the condition for thermal equilibrium is reduced to $\partial L_r / \partial q = 0$ for the accreted envelope in the high density, where ϵ_r is much larger than $\epsilon_g^{(h)}$ because of the high conductivity of degenerate matter. In this case, the thermal structure of the envelope is determined by the heat flow from the inner part and/or by the gravitational energy release of accreted material at the outer shell where electrons are not degenerate. In such an envelope, the nuclear shell burning makes a thermal runaway when the bottom of the accreted envelope reaches the state where the condition $F > 0$ is satisfied. Therefore, the equation $F = 0$ gives the ignition point of shell flashes.

b) Stability of Hydrogen and Helium Shell Burnings

In our computations, the same radii as Hansen and Van Horn (1975) are used for comparisons with other works, although some uncertainties remain concerning

the radius of a neutron star (see e.g., Baym and Pethick 1979). Nuclear reaction rates are taken from Fowler, Caughlan, and Zimmerman (1975), and screening corrections to them are taken from Graboske *et al.* (1973) and Itoh, Totsuji, and Ichimaru (1977). The radiative opacities are taken from Cox and Stewart (1970), and for the conductive opacities, Iben's (1975) analytic approximations to the results of Hubbard and Lampe (1969) and of Canuto (1970) are used. We assume the chemical compositions of $X = 0.73$, $Y = 0.25$, and $Z = 0.02$ (all composed of CNO elements) for the accreted material.

Results are shown on ΔM -temperature diagrams of Figures 1 and 2 in the case of neutron stars with a mass of $M = 0.476$ and $1.41 M_\odot$, respectively. Thick lines (solid and broken) denote the loci where the thermal equilibrium condition of equation (6) is satisfied for hydrogen burning. In the right-hand side of these lines, the energy generation rate per unit mass due to hydrogen burning ϵ_H overweighs the heat diffusion rate ϵ_r , so that the temperature of the shell rises as a result of nuclear heating. Hatched areas represent the region where F in equation

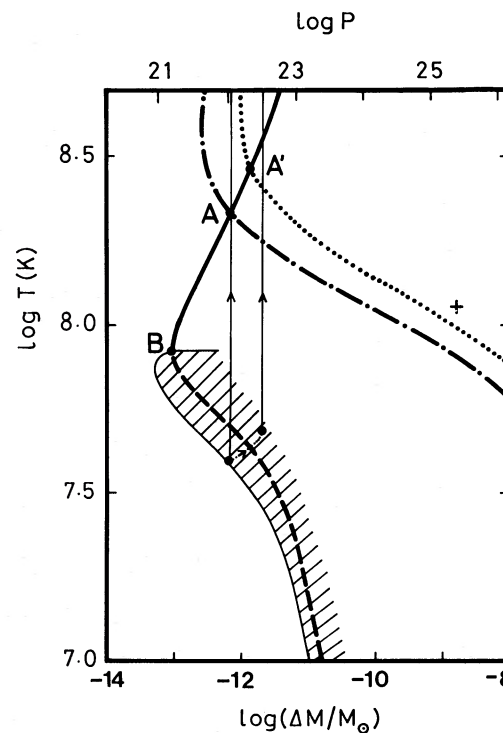


FIG. 1.—Stability conditions for shell burnings are plotted on the diagram of the envelope mass ΔM and temperature T for $M = 0.476 M_\odot$. Solid and dashed parts of the thick line show the condition of stable and unstable hydrogen burnings under the thermal equilibrium. This line corresponds to the bottom of the hydrogen-burning shell. The hatched area represents the unstable region for hydrogen burning against perturbations of the first order ($F > 0$). Dash-dotted and dotted lines denote the ignition lines ($F = 0$) for helium burning in the cases of $Y = 1.0$ and 0.25 , respectively. For points A , A' , and B , see text. Evolutionary paths computed by Taam and Picklum (1979) are shown by thin lines with their boundary condition designated by the cross.

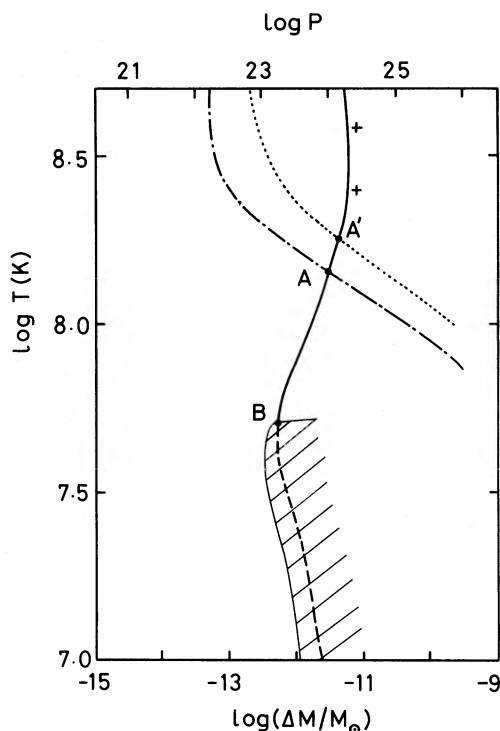


FIG. 2.—Same as Fig. 1 but for $M = 1.41 M_{\odot}$. Crosses denote the inner boundary conditions for models computed by Joss (1978).

(9) is positive for hydrogen burning. For helium burning, we show the ignition lines given by $F = 0$ in cases of $Y = 1.0$ and 0.25 by dash-dotted and dotted lines, respectively.

We see from these Figures 1 and 2 that hydrogen-shell burning becomes thermally stable where the temperature is $\log T(\text{K}) \gtrsim 8.0$ (7.7) for $M = 0.476$ (1.41) M_{\odot} (points designated by symbol B). This is because the temperature dependence ν_{H} of ϵ_{H} is reduced to a very small value owing to the saturation of CNO cycles by β -decays. In Figures 1 and 2, the stable branch (solid lines) has the opposite slope to the unstable part (broken lines). From equations (6) and (7), we see that the higher temperature, hydrogen-burning shell has higher density in a thermal equilibrium when $\nu_{\text{H}} < 4 - \kappa_{\text{T}}$. In our models, therefore, the bottom of the stable hydrogen-burning shell is forced to lie at a density as high as $\log \rho \approx 4.9$ – 5.6 (6.3 – 6.9) for 0.476 (1.41) M_{\odot} . Because of high temperature and high density, the loci of a stable hydrogen-burning shell crosses even the ignition lines of helium burning for $Y = 1.0$ and 0.25 at points A and A' , respectively.

We summarize the values of \dot{M}_{st} defined in equation (8) for the hydrogen burning at points A and B , i.e., $\dot{M}_{\text{st}}(A)$ and $\dot{M}_{\text{st}}(B)$, in Table 1. Once ignited, the bottom of the hydrogen-burning shell reaches this stable branch and settles down there unless the helium-shell flash is ignited. Then materials are processed at the rate \dot{M}_{st} . On the other hand, the accretion replenishes the nuclear fuel from the surface. When they balance each other, the mass of the

TABLE 1
PARAMETERS OF NEUTRON STARS AND
ACCRETION RATES

M/M_{\odot}	$R(\text{km})$	\dot{M}_{cri}^a	$\dot{M}_{\text{st}}(A)^a$	$\dot{M}_{\text{st}}(B)^a$
0.476	8.67	15	0.46	0.046
1.00	7.49	13	1.0	0.31
1.41	6.57	12	1.9	0.27

^a \dot{M} is given in units of $10^{-9} M_{\odot} \text{ yr}^{-1}$.

hydrogen-rich envelope ΔM_{H} no longer changes, and the steady state shell burning is realized. If more hydrogen is consumed by the nuclear burning than supplied by the accretion, i.e., $\dot{M} < \dot{M}_{\text{st}}$, the hydrogen-rich envelope becomes thin in mass, and the bottom of it shifts outward along the locus of this stable branch. After it passes through point B , the nuclear burning is extinguished since the nuclear energy generation rate ϵ_{H} after that point becomes smaller than the heat diffusion rate ϵ_{T} . As a corollary, the accretion rate greater than $\dot{M}_{\text{st}}(B)$ is the necessary condition to maintain the stability of the hydrogen-shell burning. When $\dot{M} > \dot{M}_{\text{st}}$, on the contrary, the burning shell is pushed deeper along the stable branch. If \dot{M} is still larger than $\dot{M}_{\text{st}}(A)$, the bottom of the accreted envelope will merge into the unstable region of helium burning before the hydrogen-shell burning settles in a steady state.

In the case of helium-shell burning, such a steady-state configuration will not be realized. It is true that the temperature dependence of the 3α reaction becomes smaller than 4 for $\log T > 8.8$, but at such a high temperature, helium is depleted very rapidly. Therefore, in order to keep such shell burning stationary, the supply of helium calls for the accretion rate to be even greater than the critical value \dot{M}_{cri} limited by Eddington luminosity.

As seen from equations (6) and (7), the dependences on the mass and radius of a neutron star are included only through the pressure scale height H_p , which is in inverse proportion to the surface gravity g of a neutron star. Larger gravity compels the nuclear burning shell to higher density, i.e., $\Delta \log \rho \approx [2(\partial \ln P / \partial \ln \rho)_T + \kappa_{\rho} + \eta]^{-1} 2\Delta \log g$. This effect is the most remarkable for the stable branch of the hydrogen-burning shell because of $\eta \approx 0$. The lowest temperature of this stable branch, i.e., that at point B , decreases since the CNO cycles are saturated at lower temperature for higher density. For helium burning, this effect is small because of the strong dependence on density, i.e., $\eta > 2$. Consequently, the temperature of point A also decreases in the case of a neutron-star model with higher gravity. If the surface gravity is larger than our case of $M = 1.41 M_{\odot}$, the density at the hydrogen-burning shell would exceed the threshold for electron capture on protons.

Although we have discussed the hydrogen and helium shell burnings separately, some helium may burn to produce ^{12}C in the stable hydrogen-shell burning especially near point A because of high density and high temperature. Newly produced ^{12}C enhances the energy

generation rate through CNO cycles and causes the increase in the temperature of the stable branch T_H (Taam and Picklum 1978). Since T_H depends on the abundance of CNO elements Z_{CNO} as $\delta \ln T_H = [4 - \kappa_T]^{-1} \delta \ln Z_{\text{CNO}}$, the time scale of the rise in T_H caused by this helium-burning τ_{ris} can be computed from

$$\tau_{\text{ris}} \equiv dt/d \ln T_H = [4 - \kappa_T] Z_{\text{CNO}} E_{\text{He}} \Delta M_H / L_{\text{He}} \quad (10)$$

and gives $\tau_{\text{ris}} = 2.3(1.6) \times 10^3 (Z_{\text{CNO}}/0.02)$ s at point A for $M = 0.476(1.41) M_\odot$. The τ_{ris} is shorter than the time scale of hydrogen depletion in the shell

$$\begin{aligned} \tau_{\text{dep}} &\equiv dt/d \ln X = X E_H \Delta M_H / L_H \\ &= 3.5 \times 10^4 (0.02/Z_{\text{CNO}}) \text{ s}; \end{aligned}$$

nevertheless, they are much longer than the time scale of heat diffusion $\tau_r \equiv c_p T / \epsilon_r = 3.4(1.3) \times 10^2$ s in the shell. This implies that the effect of this helium burning is to make the loci of the stable branch shift upward to a higher temperature; therefore, the upper limit to the envelope mass ΔM_H of steady-state hydrogen-shell burning is smaller than that in Figures 1 and 2. However, the decrease in the envelope mass is small because of the strong dependence of τ_{ris} on ΔM_H , i.e., $d \log \tau_{\text{ris}} / d \log \Delta M_H \approx 10(20)$. Moreover, it is to be noticed that the upper limit to the accretion rate for the steady-state hydrogen-burning $\dot{M}_{\text{st}}(A)$ is made larger than in Table 1, since the increase in ϵ_H overtakes the decrease in ΔM_H in equation (3).

An anonymous referee kindly pointed out the possibility of electron captures of ^{14}O and ^{15}O for the case of $1.41 M_\odot$ because of high density. Such electron captures bypass the β -decays and shorten the round time of the CNO cycle. The nuclear reaction rate, however, is enhanced by this shortening of the round time only twice, since the capturing rates of both reactions are on the order of β -decays (~ 100 s), even for the case of $\log \rho (\text{g cm}^{-3}) = 6.9$ and $\log T (\text{K}) = 9$. As these reactions work at a high density and high temperature, such enhancement of ϵ_H decreases the mass of points A and A' somewhat ($\delta \log \Delta M \sim -0.1$) and increases the burning rate $\dot{M}_{\text{st}}(A)$ ($\delta \log \dot{M}_{\text{st}} \sim 0.2$).

c) Three Paths for Shell Burning

We can classify the progress of nuclear shell burnings into the following three cases according to the accretion rate. They are discriminated by the situation of hydrogen-shell burning. To clarify the following discussions, evolutionary loci of each case are illustrated schematically in Figure 3.

First we discuss the case when hydrogen burns on the stable branch. It requires the accretion rate \dot{M} to be greater than $\dot{M}_{\text{st}}(B)$. If \dot{M} is even larger than $\dot{M}_{\text{st}}(A)$, the bottom of the accreted envelope is pushed into the unstable region of helium-burning before all hydrogen is depleted. Consequently, the helium-shell flash proceeds accompanying proton captures on nuclear products of helium burning. We call this *case 1*. Because of the high accretion rate in this case, the effects of the accreting flow

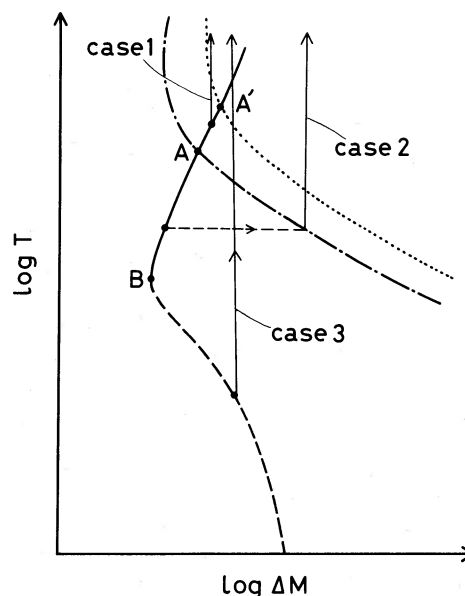


FIG. 3.—Progresses of shell flashes for three cases are illustrated schematically in the same diagram as Figs. 1 and 2. The thin dashed line denotes the evolutionary locus of the bottom of the accreted envelope after the hydrogen-burning shell.

are significant for observational properties of shell flashes, which we shall discuss in § IVb.

In the case of an intermediate accretion rate, i.e., $\dot{M}_{\text{st}}(A) > \dot{M} > \dot{M}_{\text{st}}(B)$, the hydrogen-shell burning settles in a steady state between points A and B . This is called *case 2*. Then, the mass of the hydrogen-rich envelope ΔM_H remains constant, and the accreted material is processed at the same rate as it is accreted. As a result, the helium zone is formed below the hydrogen-burning shell and grows in mass. Even if the core of the neutron star has been cooled down beforehand, the helium zone is heated up by the inward heat flow from the hydrogen-burning shell. Since the time scale of heat diffusion in the helium zone is much shorter than that of helium accumulation, the isothermal structure is realized with a temperature equal to that of the hydrogen-burning shell T_H . The evolutionary locus at the bottom of the accreted envelope in this stage is illustrated by the thin dashed line in Figure 3. When the mass of the helium zone reaches the critical value where the isothermal line of T_H crosses the ignition line of $Y = 1.0$, the helium-shell flash is triggered.

If the accretion rate is smaller than $\dot{M}_{\text{st}}(B)$, the hydrogen-shell burning is extinguished during the inter-flash phase. In *case 3*, therefore, the hydrogen burning is ignited at the lower temperature, unstable branch after the increase in the mass of the hydrogen-rich envelope by the accretion. Then, the hydrogen-shell flash heats up the layer at least to the temperature of the stable branch. The amount of hydrogen consumed before reaching the ignition point ($F = 0$) is estimated from

$$\begin{aligned} \Delta X &= L_H^{(i)} / E_H \dot{M} \approx 0.010 (L_H^{(i)} / 0.1 L_\odot) \\ &\quad \times (\dot{M} / 10^{-10} M_\odot \text{ yr}^{-1})^{-1}, \quad (11) \end{aligned}$$

where $L_H^{(i)}$ denotes the hydrogen-burning rate when the bottom of the accreted envelope reaches the ignition point. It is a decrease function of the temperature at the ignition point T_i and as small as $L_H^{(i)} \approx 0.014(0.15) L_\odot$ even at $T_i = 10^7$ K for $0.476(1.41) M_\odot$. For the heating after ignition, the burning of only a fraction of hydrogen is sufficient, i.e.,

$$\Delta X = \frac{c_p \Delta T}{E_H} \approx 0.002 \left(\frac{c_p}{10^8 \text{ ergs g}^{-1} \text{ K}^{-1}} \right) \left(\frac{\Delta T}{10^8 \text{ K}} \right). \quad (12)$$

If the mass of the accreted envelope is larger than that of point A' , the hydrogen-shell flash develops continuously into the helium-shell flash with the helium concentration as small as that in the accreted gas. This evolutionary locus is illustrated in Figure 3. Otherwise, the burning shell settles once it is on the stable branch, and the initiation of the helium-shell flash awaits the accumulation of some helium and/or the increase of CNO elements due to the 3α reactions which cause the hydrogen-burning to raise the temperature of the burning shell. As a consequence, the helium-shell flash proceeds in the bath of protons as in case 1, although the blend of helium and hydrogen depends on the thermal history before the ignition of the hydrogen-shell flash.

From equation (11), it may be seen that the hydrogen is depleted before the ignition at the bottom of the accreted envelope if T_i is higher than 10^7 K and the accretion rate is smaller than $\dot{M} = 1.9(21) \times 10^{-13} M_\odot \text{ yr}^{-1}$ for $M = 0.476(1.41) M_\odot$. However, this is not true usually since such a high T_i necessitates a still higher temperature at deeper layers which is anticipated only for an accretion rate larger than $\dot{M}_{st}(B)$, as is discussed in § IVc. When the accretion rate decreases from a value larger than $\dot{M}_{st}(B)$ to such a small one, the envelope is cooled down immediately after the decrease because of the very short time scale of heat diffusion ($< 10^5$ s).

We have so far considered shell flashes during recurrences. The hydrogen-shell burning is extinct, however, before the onset of the accretion event or during the interruption. Therefore, the first shell flash after the start or the resumption of accretion will be triggered at the unstable branch of hydrogen-burning, as in case 3, even if the accretion rate is larger than $\dot{M}_{st}(B)$. The cases computed by Taam and Picklum (1979) correspond to this case.

III. PROGRESS OF HELIUM-SHELL FLASHES

In an accreting neutron star, the helium-shell flash has two characteristic features. One is variety in the concentration of helium and hydrogen at the ignition according to two different situations. In case 2, ignition is triggered in the helium zone below the hydrogen-burning shell, as in the cases of red giant stars and accreting white dwarfs. In cases 1 and 3, on the contrary, the helium-shell flash is initiated in coexistence with hydrogen and develops accompanying proton captures on nuclear products. Hereafter, we call the former case the pure helium-shell flash, and the latter the combined helium and hydrogen shell flash. Shell flashes computed by Joss (1978) and by

Taam and Picklum (1979) correspond to the former and the latter cases, respectively, although their parameter ranges are different from our cases.

Another feature of shell flashes on a neutron star is that the pressure of the burning shell P_b remains constant throughout the shell flash. Because the deep gravitational potential of the star is greater than the nuclear energy released by the shell flash, the expansion of the envelope due to the shell flash is much smaller than the radius of the neutron star, and the shell remains flat in configuration. Therefore, the temperature of the burning shell T_b continues to rise as long as the energy gain due to nuclear burning overweighs the energy loss through heat diffusion, i.e., $\epsilon_N > \epsilon_r$.

Consequently, the progress of a shell flash is determined by two parameters: the initial concentrations of hydrogen and helium (X_0, Y_0) and the pressure of the burning shell P_b . The effects of difference in the mass of the neutron star are restricted only to the onset and the final stage, when heat diffusion plays an important role. Therefore, such difference in mass has little influence on the progress of a shell flash itself except for the case of lower pressure, weak flashes, such as $\log P_b \approx 22.0$ and 22.5 for $M = 0.476$ and $1.41 M_\odot$, respectively.

In order to investigate the progress of shell flashes, we follow numerically the changes in chemical compositions owing to nuclear reactions. As we are interested mainly in the strength of a shell flash, we have simplified the process of nuclear reactions. For the thermodynamics of the shell, the same approximations as in § II are used, and uniformity of abundances in the envelope is assumed since the bulk of the envelope is to be incorporated into the convective zone during shell flash. The time variations of quantities are computed from the variation of specific entropy s in the convective zone, i.e.,

$$\langle T \rangle \frac{ds}{dt} = \frac{L_N}{\Delta M}, \quad (13)$$

where $\langle T \rangle$ is an averaged temperature in the convective zone and is given by

$$\langle T \rangle \equiv \frac{1}{\Delta M} \int_M^{M+\Delta M} T dM_r = \left[1 + \frac{1}{n+1} - \frac{4}{V} \right]^{-1} T_b. \quad (14)$$

Equation (13) holds good as long as the nuclear energy generation rate L_N is larger than the radiative energy loss from the surface. Our computations start at the stage when the energy generation rate due to 3α reaction $\epsilon_{3\alpha}$ becomes greater than ϵ_r and when $\epsilon_{3\alpha} \gtrsim \epsilon_H$ in the case of $X_0 > 0$. They are continued until ϵ_N is reduced smaller than ϵ_r again. We discuss cases of the pure helium-shell flash and of the combined helium and hydrogen shell flash in §§ IIIa and IIIb, respectively.

a) Pure Helium-Shell Flashes (Case 2)

Joss (1978) computed models with relatively low pressure of $\log P_b = 22.6$ and 23.1 for a $1.41 M_\odot$ neutron star. However, we see from Figure 2 that shell flashes take place even under much higher P_b , and we shall discuss the

dependence of their strength on P_b . We assume the initial abundance of helium $Y_0 = 1.0$, for simplicity, and take into account the 3α reaction and $^{12}\text{C}(\alpha, \gamma)^{16}\text{O}$. Because of high density, the latter reaction operates at temperatures higher than 10^9 K, as verified by computations below, and then α -captures of ^{16}O , ^{20}Ne , and ^{24}Mg proceed much faster than it. Therefore, we assume that it is followed immediately by captures of three more α -particles to synthesize ^{28}Si . Above 10^9 K, ^{28}Si and heavier elements may also react faster than ^{12}C . Because the binding energy of ^{28}Si is large enough, however, neglecting the further process of α -captures will little effect our results.

Results are summarized in Figure 4 in the cases of different P_b for $M = 1.41 M_\odot$; the variation of the nuclear energy generation rate L_N and the nuclear heating time scale in the convective zone $\tau_h \equiv dt/d \ln T_b = c_p \langle T \rangle \Delta M / L_N$ are plotted against the increase in temperature of the burning shell T_b .

The shell flash proceeds as follows. At first, it is driven by 3α reaction. Although it becomes saturated as T_b approaches to 10^9 K, the high density of the burning shell

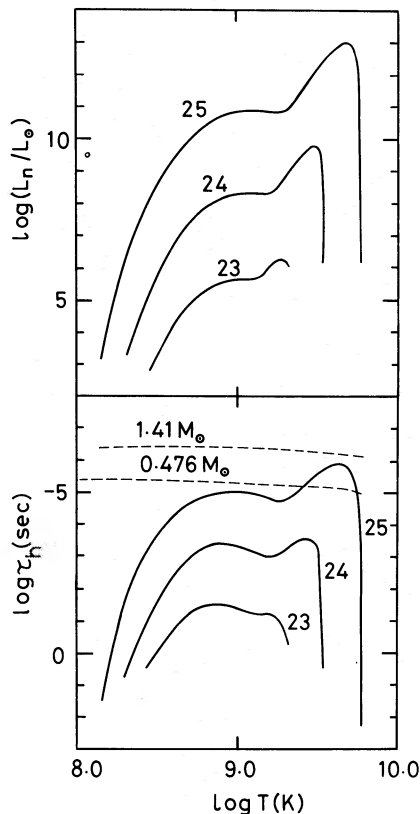


FIG. 4.—Time variations of the nuclear energy generation rate L_N (top) and the nuclear heating time scale τ_h (bottom) during pure helium-shell flash for $M = 1.41 M_\odot$. For abscissa, the temperature at the bottom of the burning shell T_b is taken instead of time. Each curve corresponds to a different pressure of the burning shell P_b , to which the value of $\log P_b$ is attached. Dynamical time scales τ_{dyn} are shown by dashed lines for $M = 0.476$ and $1.41 M_\odot$ of $\log P_b = 25.0$.

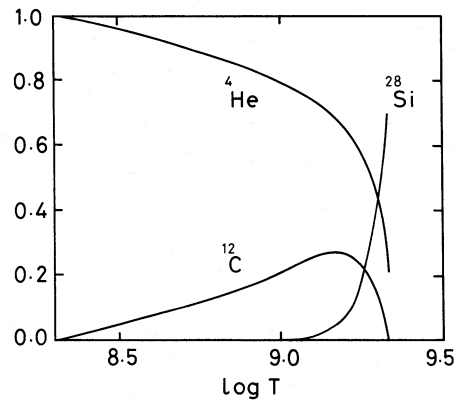


FIG. 5.—Changes in chemical composition mass concentration during shell flashes for a pure helium-shell flash in the case of $\log P_b = 23.0$.

still yields a large burning rate $\epsilon_{3\alpha}$. Therefore, the operation of $^{12}\text{C}(\alpha, \gamma)^{16}\text{O}$ reaction is postponed until T_b becomes higher than 10^9 K. During this course, carbon is accumulated, and its concentration amounts to a fourth in mass. Thereafter, α -capture reactions enhance the nuclear energy generation rate because of its strong temperature dependence and bring L_N to a maximum value L_N^{max} . The progress of reactions is seen in Figure 5, which shows the variation of chemical compositions during the shell flash.

As T_b rises, the radiation pressure becomes important. When T_b approaches the critical value limited by the radiation pressure $T_{\text{lim}} \equiv (3P/a)^{1/4}$, the density tends to vanish (Sugimoto and Nomoto 1975). In this case, the increase in specific heat capacity c_p by the contribution of the radiation field is more important. When c_p becomes greater than $E_N X_N / T_b$, nuclear fuels begin to be depleted faster than T_b rises, which reduces ϵ_N to a value smaller than ϵ_r . Then, T_b reaches its maximum T_b^{max} and tends to decrease. Therefore, shell flash is quenched when the contribution of the gas pressure to total (gas plus radiation) pressure β becomes as small as $\beta = 0.5 \sim 0.7$. Because of high T_b at this stage, all carbon constructed by 3α reaction is converted into elements heavier than ^{28}Si , as argued by Joss (1978).

As seen from Figure 4, L_N^{max} is much larger than the Eddington luminosity $L_{\text{cri}} \equiv 4\pi GcM/\kappa_{\text{el}}$ (κ_{el} is the electron-scattering opacity) in spite of the very small envelope mass, and τ_h is reduced to much smaller than 1 second. Because of large L_N^{max} as compared to the envelope mass, the duration of the shell flash is also very short ($E_N \Delta M / L_N^{\text{max}} \lesssim 0.1$ s).

We see also that the strength of shell flash depends strongly on P_b ; if P_b is higher, L_N reaches a much larger value, τ_h is reduced to a much smaller value, and the value of T_b^{max} is higher. In the case of $\log P_b = 25.0$, τ_h becomes even smaller than the dynamical time scale of the envelope τ_{dyn} for $M = 0.476 M_\odot$, which is necessary for sound waves to travel over the pressure scale height, i.e., $\tau_{\text{dyn}} \equiv H_p(\rho/P)^{1/2}$. In this case, a shock wave is formed which propagates and causes dynamical phenomena on the surface of the neutron star. For still higher P_b , the

shock may be strong enough to develop into a detonation wave. For $M = 1.41 M_{\odot}$, such phenomena take place in the case of slightly higher P_b because of smaller H_p .

The nuclear energy released during shell flash is transported to the stellar surface and raises the surface luminosity close to L_{cri} as far as $L_N^{\text{max}} > L_{\text{cri}}$. Although we consider only quantities at the burning shell, we can deduce the observational relevance of our results since the very short τ_h is related to the rapid rise of surface luminosity in the following way. In the thin envelope of a neutron star, the entropy barrier between the photosphere and the burning shell is smaller than the entropy generated by nuclear burning, as long as the accreting flow is optically thin. Therefore, the extension of the convective zone is limited not by the entropy barrier but by the heat diffusion because the time scale of heat diffusion τ_r is very small at the photosphere. Then, the convection extends outward through the layer where τ_r is comparable with τ_h at the peak stage $\tau_h^{(p)}$ (Fujimoto 1977). It implies that the surface luminosity reaches its maximum value in a time scale of $\tau_h^{(p)}$, and by the same time scale behind the peak of shell flash.

Consequently, the pure helium-shell flash reproduces the correct order of rise time and duration of the fast mode. For higher pressure, i.e., $\log P_b > 25.0$, the shock wave would produce a steeper rise and higher surface luminosity than L_{cri} . The detonation wave would lead to the heating up of the surface layer to the temperature necessary to produce γ -ray photons by the dissipation of kinetic energy (Woosley and Taam 1976).

Finally, we discuss the effects of the overlying hydrogen-rich layer. As in the case of accreting white dwarfs (Fujimoto and Sugimoto 1979b), the helium convective zone may reach the bottom of the hydrogen-rich layer. Then, protons are mixed down to the shell where the lifetime against reactions $^{12}\text{C}(p, \gamma)^{13}\text{N}(p, \gamma)^{14}\text{O}$ is comparable to the convective mixing time scale. The additional nuclear energy from this reaction might lead to the separation of the convective zone, as shown by Sugimoto *et al.* (1978) in the case of accreting white dwarfs. This has two effects on the further progress of the shell flash: (1) it shortens somewhat the nuclear heating time scale and expels the convective zone farther outward than in the case of only helium-shell burning, and (2) the entropy barrier produced between the two convective zones prevents further dilution of hydrogen by helium convection, making it possible for the hydrogen layer to survive the shell flash. The latter effect is important to the investigation of the succeeding interflash phase and the recurrence of shell flashes.

b) Combined Helium and Hydrogen Shell Flashes (Cases 1 and 3)

When helium and hydrogen coexist, the process of helium-burning is modified by proton captures. Such situations were first considered by Taam and Picklum (1979). The nuclear products immediately capture protons and become unstable nuclei. Because of the short heating time scale, β -decays of such nuclei are bypassed

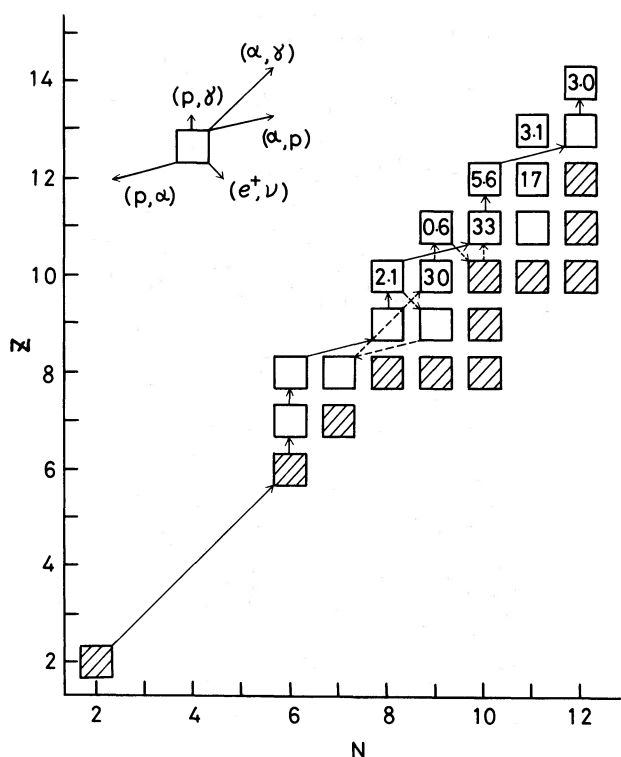


FIG. 6.—Illustration of nuclei considered for combined helium and hydrogen shell flash. Solid and dashed arrows denote the paths used in our computations. Hatched squares represent stable nuclei, and numerals in open squares designate the lifetime against β -decay.

through (α, p) reaction. Therefore, the rising phase and the peak of the shell flash are determined by the strong interactions, except for the weak flashes. We illustrate the process of nuclear reactions in such situations in Figure 6.

In order to estimate the strength of shell flashes, in Figure 6 we follow the 3α reaction and plausible process of α -captures up to ^{26}Si with additional energy releases through proton captures (path is indicated by solid lines). Reaction rates are taken from Wagoner, Fowler, and Hoyle (1967). Although these rates are subject to considerable uncertainty, our computation provides insight into the progress of combined helium and hydrogen shell flashes.

We compute two cases of initial compositions with $(X_0, Y_0) = (0.48, 0.5)$ and $(0.73, 0.25)$, the latter of which is taken equal to the compositions in the accreted material. Results are shown in Figure 7 for the case of $\log P_b = 23.0$ for $M = 0.476 M_{\odot}$. The value of P_b is higher than in models computed by Taam and Picklum (1979), where $\log P_b = 22.1$, and 22.6. For comparison, we also plot in Figure 7 results of a pure helium-shell flash with the same pressure. Variations of chemical compositions in our computations are also shown in Figure 8.

We see from Figure 7 that, for smaller Y_0 , the shell flash is weaker; i.e., L_N is smaller and τ_h remains longer. This relation is ascribed mainly to the strong dependence of

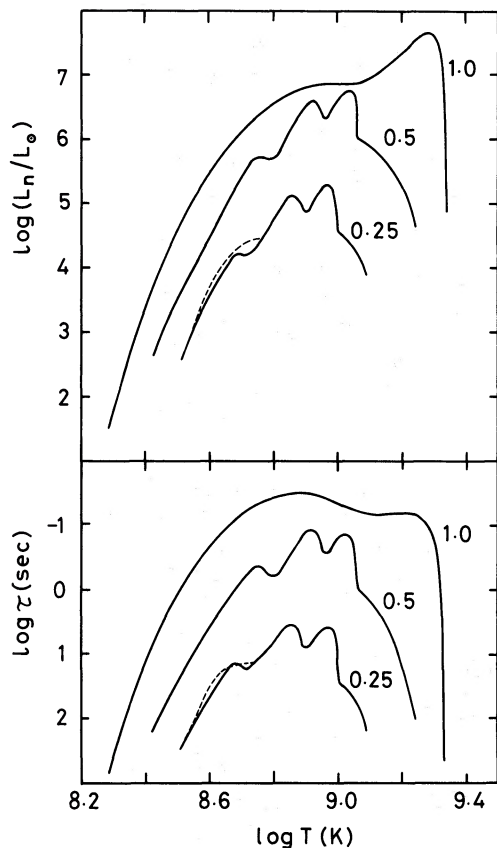


FIG. 7.—The same as Fig. 4 but for combined helium and hydrogen shell flashes in the case of $\log P_b = 23.0$, and $M = 0.476 M_\odot$. Results for a pure helium-shell flash are also shown for comparison. The initial concentration ratio of helium Y_0 is indicated for each curve.

the 3α reaction on the helium abundance Y , i.e., $\epsilon_{3\alpha} \propto (1 + X)^{-2} Y^3$. It also leads to the operation of α -capture reactions at a lower temperature for smaller Y_0 . The reaction of ^{14}O proceeds at a much lower temperature than $^{12}\text{C}(\alpha, \gamma)^{16}\text{O}$ and before the concentration of ^{14}O amounts appreciably. As its temperature dependence is stronger than that of 3α reaction, the abundance of ^{14}O decreases rapidly, as seen in Figure 8. Therefore, the maximum abundance amounts only to a few percent, so that it yields only a small hump on the curves of L_N and τ_h . Thereafter, the reaction of ^{14}O is controlled by the production rate of ^{12}C through 3α reaction. Reactions of ^{18}Ne and ^{22}Mg proceed in the same way and yield humps on L_N and τ_h , successively. We see that the top of the humps saturates above $\log T_b \gtrsim 8.9$, mainly as a result of the saturation of the 3α reaction.

In the case of $Y_0 = 0.25$, therefore, the nuclear heating time scale at the peak stage $\tau_h^{(p)}$ gives an order of several seconds, which is characteristic of the rise time of the slow mode. In the case of $Y_0 = 0.5$, however, the shell flash is strong enough to reduce $\tau_h^{(p)}$ to smaller than a tenth of a second. For higher P_b , the shell flash is also stronger, as discussed in the case of a pure helium-shell flash. If log

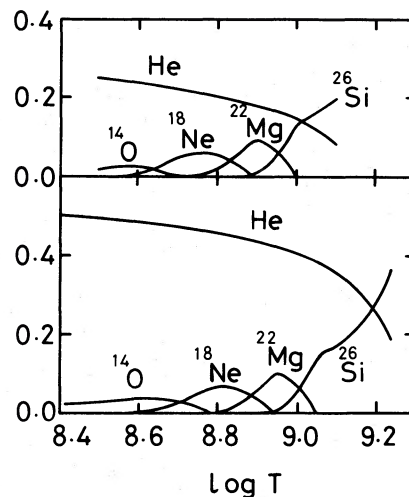


FIG. 8.—The same as Fig. 5 but for a combined helium and hydrogen shell flash.

$P_b \gtrsim 24.0$, $\tau_h^{(p)}$ becomes shorter than a tenth of a second even for $Y_0 = 0.25$.

For a weak shell flash, decay of ^{18}Ne to ^{18}F may proceed faster than α -particle capture on ^{18}Ne at low temperature ($\log T_b < 8.75$). Then, reactions proceed as indicated by the broken lines in Figure 6. Taking this process into account, however, little changes the characteristics of shell flash shown for the case of $Y_0 = 0.25$ in Figure 7.

After the exhaustion of helium, proton captures on the nuclear products of helium burning and resultant β -decays may still keep the nuclear energy generation rate high. From the characteristic lifetime τ_β against β -decay and from the number of α -particles which produce seed nuclei for proton captures N , we can estimate the nuclear energy generation rate at this stage as $L_N = 2 \times 10^5 / N \tau_\beta (Y_0 / 0.25) (\Delta M / 10^{-12} M_\odot) L_\odot$, assuming half of the nuclear energy is lost through neutrinos. If $L_N \gtrsim L_{\text{cri}}$, the surface luminosity remains close to L_{cri} and broadening of burst profile occurs. The progress of this process is determined by the lifetime of β -decays of proton-rich unstable nuclei; it takes about 10–20 seconds to synthesize iron-peak elements from elements like ^{26}Si .

In the case of $Y_0 = 0.5$, plenty of helium is left after ^{26}Si is produced, so that α -capture proceeds further to heavier elements. If seed nuclei for proton captures are depleted, the energy generation rates will be reduced, and the duration of shell flash becomes short. Consequently, combined shell flashes produce a variety of rise times and durations, depending on the initial helium abundance Y_0 and P_b . In the case of Y_0 as small as 0.25 and $\log P_b$ lower than 24.0, we can expect the rise time and the duration of X-ray burst characteristic to the slow-mode bursts observed by Murakami *et al.* (1980a).

IV. CONCLUSIONS AND DISCUSSION

a) Conclusions

We have analyzed thermal properties of shell burnings and revealed the mechanism which ignites the helium-

shell flashes on an accreting neutron star. Based on this result, we predict three evolutionary paths of shell burnings depending on the accretion rate \dot{M} . These are case 1 for the high accretion rate, $\dot{M} > \dot{M}_{st}(A)$, when the stable hydrogen-burning shell plunges into the unstable region of helium burning; case 2 for the intermediate rate, $\dot{M}_{st}(A) > \dot{M} > \dot{M}_{st}(B)$, when the hydrogen-shell burning stays in a steady state, and the helium-shell flash is triggered in the helium zone below the hydrogen shell; and case 3 for the low accretion rate, $\dot{M} < \dot{M}_{st}(B)$, when the hydrogen-shell flash develops into the helium-shell flash. In all of these cases, the helium-shell flash is ignited even when the core has been cooled down.

As a natural consequence, the helium-shell flash is triggered when helium coexists with hydrogen in various degrees of concentration. In case 3, the helium abundance at the onset stage of the helium-shell flash is as small as the initial value in the accreted material. In case 2, on the contrary, all hydrogen is depleted at the bottom of the accreted envelope before the ignition of the helium-shell flash.

Helium-shell flashes result in the various time scales appropriate to type I X-ray bursts of different modes, depending on the degree of the blend of helium and hydrogen and on the pressure of the burning shell P_b . When the shell has a large helium abundance, the flash is sharp enough to make the burst profile of the fast mode. In the case of $\log P_b \gtrsim 25.0$, it even triggers the dynamical phenomena on the neutron star. When the helium abundance is as small as $Y_0 = 0.25$ and $\log P_b < 24.0$, the resultant shell flash is comparatively dull and reproduces the rise time and the duration of the order observed for bursts of the slow mode.

On a neutron star, the thickness of the envelope ΔR is much smaller than the radius R , i.e., $\Delta R/R = [(N+1)/V]_b \ll 1$. Therefore, the shell flash seems to be triggered only in part of the envelope and not simultaneously in the whole envelope, as is also suggested by the recurrence period (see below). Although we have assumed spherical symmetry of the envelope in our analysis, it is reduced to plane symmetry, as seen in equation (2). This implies that our results can also be applied to such situations as long as the scale of the burning region D is sufficiently larger than the thickness of the envelope ($D \gg \Delta R$). In this case, quantities such as the luminosity should be renormalized with the dimension of the burning region instead of with the whole surface of a neutron star, i.e., reduced by a factor of $D^2/4R^2$.

b) Relevance to Observations

There exist X-ray bulge sources which seem to belong to the same category of accreting neutron stars as X-ray burst sources. These bulge sources show the same characteristics as the burst sources, except for the existence of type I X-ray bursts (Lewin and Joss 1977). Here we argue that case 1 shell flashes correspond to these bright bulge sources and that cases 2 and 3 shell flashes correspond to bursts of the fast and slow modes, respectively.

i) Disappearance of X-ray Bursts

Observational properties of shell flashes depend directly on the state of the surface layer of the accreting neutron star. As long as the accreting flow is optically thin at the low accretion rate, the gravitational energy released by the infalling material is radiated away before it reaches the photosphere and has little effect on the thermal structure of the outer envelope. Then, shell flashes produce type I X-ray bursts, as shown in computations by Joss (1978) and by Taam and Picklum (1979), both neglecting the effects of accreting flow on the surface layer.

If the accretion rate is high enough to make the infalling flow optically thick, however, the situation is quite different. The thermal structure of the outer envelope suffers crucial changes: the entropy of the photosphere increases significantly through the dissipation of the kinetic energy of infalling material, so that the photosphere expands to be as large as the radius of the neutron star. The progress of the shell flash itself has nothing to do with the infalling material because of the higher pressure of the burning shell. However, the observational properties of the shell flashes are deeply affected. The large entropy barrier between the photosphere and the burning shell prevents the extension of the convective zone, and a large radiative zone may be left between the photosphere and the top of the convective zone. Travel of photons over this distance will delay and blur the rise of surface luminosity due to the shell flashes.

A sequence of such events is expected when the electron-scattering optical depth in the infalling flow is greater than unity. Assuming the free fall, it is reduced to the condition for the accretion rate as

$$\dot{M} \gtrsim 4.7 \times 10^{-9} \left(\frac{R}{10^6 \text{ cm}} \right)^{1/2} \left(\frac{M}{M_\odot} \right)^{1/2} M_\odot \text{ yr}^{-1}. \quad (15)$$

This range covers almost all of the part of the accretion rate in case 1 for $M = 1.41 M_\odot$ and the upper half for $M = 0.476 M_\odot$. The lower boundary is approximately a fifth to a third of the critical accretion rate \dot{M}_{crit} corresponding to Eddington luminosity. Because of this high accretion rate, the persistent X-ray luminosity from accretion is still close to the Eddington luminosity. Coupled effects of this persistent high luminosity and the delayed photon diffusion would be expected to mask shell flashes behind the sporadic variations of surface luminosity.

This argument is compatible with observations that bulge sources without X-ray bursts have larger persistent X-ray luminosity than X-ray bursters and that they also show large fluctuation, by a factor of 3, of X-ray flux (Hakucho team 1980). We can also explain in this way the interruption of burst activity with the increase of the accretion rate observed for MXB 1920–30 (Clark *et al.* 1977).

ii) Transitions between Two Modes

Taking into account the masking effect of the accreting flow, bursts of the slow mode are characteristic of case 3. Therefore, we can interpret the transition of a burst

profile from the fast to slow mode in terms of the decrease in the accretion rate. The transition was observed in 1608–522, and the persistent X-ray luminosity from the accretion was also observed to decrease simultaneously with these transitions (Murakami *et al.* 1980a). Moreover, the energetics of bursts is consistent with our interpretation. It is characterized by the ratio α of persistent X-ray luminosity to time-averaged burst luminosity, which, in the case of the shell-flash model, is reduced to the ratio of the gravitational potential on the surface of a neutron star to the nuclear energy released during shell flash (Lamb and Lamb 1978). In the case of the slow mode, the available nuclear energy is about 5 times larger than for the fast mode owing to the contribution of hydrogen, so that α is smaller by as much for slow mode. We can see this decrease in α for the slow mode from the observations by Murakami *et al.* (1980a).

As for other properties, such as peak luminosity and total energy release in each burst, however, we might take into account the difference in the dimension of the burning region, as mentioned below. Here, we note only that the mass of the accreting envelope necessary to trigger the helium-shell flash ΔM is dependent on the accretion rate \dot{M} . In case 2, the value of ΔM depends strongly on \dot{M} through the hydrogen-burning rate, as seen in Figures 1 and 2. In case 3, ΔM is independent of \dot{M} because the former is determined by the thermal state of the inner shell. The value of ΔM is the depth of the accreted layer. The strong dependence of ΔM on \dot{M} in case 2 will also cause the variations in dimension of the burning region corresponding to small fluctuations in \dot{M} . It may explain rather larger fluctuations in the peak luminosity observed for bursts of the fast mode, while the peak luminosity observed for bursts of the slow mode does not vary greatly (Murakami *et al.* 1980a).

iii) Recurrence Periods of Shell Flashes

As the hydrogen-burning rate is saturated by β -decays in CNO cycles, it imposes a restriction on the recurrence period of shell flashes. It takes about $190 \times (0.02/Z_{\text{CNO}})$ times of cycles for each CNO nucleus to convert all hydrogen to helium. For the distant observer, therefore, the recurrence period of shell flashes in case 2 should be greater than $3.5 \times 10^4 (0.02/Z_{\text{CNO}})(1 - 2GM/Rc^2)^{-1/2}$ s. This value gives the recurrence period at point A, as seen in Figures 1 and 2, and in Table 1. If the X-ray bursts recur in the same region, this gives the shorter limit for the interval between bursts τ_b of the fast mode.

As for the slow mode, the recurrence periods of shell flashes in the same region ought to be longer than this limit because of a smaller accretion rate. They are typically $10^6 (M/10^{-12} M_\odot)(M/10^{-10.5} M_\odot \text{ yr}^{-1})^{-1}$ and $10^6 (M/10^{-11.5} M_\odot)(M/10^{10} M_\odot \text{ yr}^{-1})^{-1}$ s for $M = 0.476$ and $1.41 M_\odot$, respectively.

According to Murakami *et al.* (1980a, b), the observed interval of bursts τ_b^{obs} seems to be, on the average, about several hours for both fast and slow modes and was observed to be as short as 10 minutes in the case of the slow mode. We may as well take the burst intervals as evidence that shell flashes take place independently and

by turn in the different parts of an envelope, rather than the whole accreted envelope burning at once. If this is the case, the average dimension of the burning region D is estimated from $D/R \sim 2(\tau_b^{\text{obs}}/\tau_b)^{1/2}$.

c) Comparisons with Other Numerical Works

We can discuss readily whole ranges of parameters owing to the semianalytical treatment. Here we discuss the relation of our results to some models constructed numerically under the specified parameters. The structure of the envelope on an accreting neutron star has been computed under the steady state approximation by Hansen and Van Horn (1975) and by Taam and Picklum (1978). In the computations of Hansen and Van Horn (1975), the structure was determined principally by the steady state condition for the helium-shell burning in deeper layers, where the concentration of helium Y is close to unity, because hydrogen is allowed to burn at an extraordinarily large rate in the outer layer where the time scale of heat diffusion is short. Therefore, their results for the helium-burning shell show good agreement with our analysis, assuming the helium accretion, although they assign much lower densities for hydrogen burning. If the proper rate of hydrogen burning is used, the temperature of envelope is determined by the hydrogen-burning shell, so that the helium-burning shell lies at a high density and spreads over density scale heights. The latter fact makes comparison with models by Taam and Picklum difficult because they give only the base of the helium zone. As for the stability analysis, the results of both works contradict ours. This difference may be ascribed to their use of the stability criterion given by Giannone and Weigert (1967), which, as was recently revealed in the case of accreting white dwarfs (see Sienkiewicz 1980), does not always give the correct results.

Evolutions of shell flashes have been computed by Joss (1978) and by Taam and Picklum (1979). In these computations, the temperatures of the inner shell are prescribed to be one of the boundary conditions (designated by crosses in Figures 1 and 2). Their results depend strongly on this boundary condition since the structure of their models before the ignition of shell flashes is determined by this boundary condition, i.e., by the heat flow from the inner shell, and independent of the accretion rate.

Pure helium-shell flashes considered by Joss (1978) would take place in case 2. We see, however, that his boundary temperatures are too high to be realized during actual evolution. Because no X-ray bursters are associated with any supernova remnant, the neutron stars of burst sources have experienced the lapse of more than 10 thousand years since their births and have been cooled down to below 10^7 K (Tsuruta 1979) before the start of the accretion events. During the accretion, the neutron star is heated up through the addition of entropy associated with the accreted gas, and the temperature of inner shells, where $\epsilon_r \gg \epsilon_g^{(h)}$ because of the high conductivity of degenerate matter, comes to be determined by this compressional heating in the outer layer where electrons are not degenerate. Because of a relatively low accretion rate,

the temperature in an accreting neutron star still remains low. The nuclear burning takes place in the accreted envelope. However, the nuclear energy released during shell flashes is readily transported away from the surface after the flash since the time scale of heat diffusion $\tau_r \equiv c_p T/\epsilon_r$ is longer for deeper layers as long as $(\partial \ln \kappa/\partial \ln P)_T > -2$, which is the condition in our case. Therefore, the shell flashes hardly contribute to the heating of the inner shell over the temperature determined by the compressional heating, as occurs in the case of helium-shell flashes in red giant stars (Fujimoto and Sugimoto 1979a). Stable hydrogen burning is the only source that can heat up the neutron star to about 10^8 K, but the temperature of stable hydrogen burning is not as high as the boundary temperatures given by Joss.

In Figure 1, we plot, by thin solid lines, the evolutionary loci taken from Taam and Picklum (1979). The ignition point for the case of an accretion rate $\dot{M} = 10^{-10} M_\odot \text{ yr}^{-1}$ is found located close to our ignition line. As stated above, the structure of the envelope is determined only by the boundary condition. When the bottom of the accreted envelope reaches the ignition line, the hydrogen-shell flash is triggered. This is the case for $\dot{M} = 10^{-10} M_\odot \text{ yr}^{-1}$. At this stage of ignition, the nuclear heating time scale of the envelope is as large as 10 thousand seconds. In the case of a high accretion rate, such as $\dot{M} = 2 \times 10^{-9}$

$M_\odot \text{ yr}^{-1}$, more mass of about $10^{-12} M_\odot$ is accumulated before the shell flash grows large in amplitude.

As the hydrogen-shell burning is extinct during the accretion, progresses of shell burnings correspond to our case 3, although the accretion rates are greater than $\dot{M}_{\text{st}}(B)$. Further evolutions of the models of Taam and Picklum (1979), therefore, would be quite different from the first flashes they computed. The hydrogen-shell burning will not be extinguished after the flash, and the hydrogen will continue stable burning thereafter. Then, evolutions after the second flashes correspond to cases 1 and 2 for $M = 2 \times 10^{-9}$ and $10^{-10} M_\odot \text{ yr}^{-1}$, respectively.

We are grateful to all the members of the *Hakucho* team at the Institute of Space and Aeronautical Science, University of Tokyo for supplying us with information regarding the observations and for discussions, to Dr. R. E. Taam for sending us his preprint, to Prof. D. Sugimoto for discussions, and to Prof. W. Unno for encouragement. M. Y. F. would like to thank Prof. I. Iben, Jr. for encouragement. Numerical computations were done at the Computer Center, University of Tokyo. This research was supported in part by the Japan Scientific Research Fund of the Ministry of Education, Science, and Culture (474109).

REFERENCES

- Baym, G., and Pethick, C. 1979, *Ann. Rev. Astr. Ap.*, **17**, 415.
 Canuto, V. 1970, *Ap. J.*, **159**, 641.
 Clark, G. W., Li, F. K., Canizares, C. R., Hayakawa, S., Jernigan, G., and Lwein, W. H. G. 1977, *M.N.R.A.S.*, **179**, 651.
 Cox, A. N., and Stewart, J. N. 1970, *Ap. J. Suppl.*, **19**, 243.
 Fowler, W. A., Caughlan, G. R., and Zimmerman, B. A. 1975, *Ann. Rev. Astr. Ap.*, **13**, 69.
 Fujimoto, M. Y. 1977, *Pub. Astr. Soc. Japan*, **29**, 331.
 Fujimoto, M. Y., and Sugimoto, D. 1979a, *Pub. Astr. Soc. Japan*, **31**, 1.
 ———. 1979b, in *IAU Colloquium 53, White Dwarfs and Variable Degenerate Stars*, ed. H. M. Van Horn and V. Weidemann (Rochester: University of Rochester), p. 285.
 Giannone, P., and Weigert, A. 1967, *Zs. Ap.*, **67**, 41.
 Graboske, H. C., DeWitt, H. E., Grossman, A. S., and Cooper, M. S. 1973, *Ap. J.*, **181**, 457.
Hakucho team, 1980, private communication.
 Hansen, C. J., and Van Horn, H. M. 1975, *Ap. J.*, **195**, 735.
 Hara, T., Ikeuchi, S., and Sugimoto, D. 1976, *Progr. Theor. Phys.*, **56**, 818.
 Hayashi, C., Hōshi, R., and Sugimoto, D. 1962, *Progr. Theor. Phys. Suppl.*, No. 22.
 Hubbard, W. B., and Lampe, M. 1969, *Ap. J. Suppl.*, **18**, 297.
 Iben, I., Jr. 1975, *Ap. J.*, **196**, 525.
 Itoh, N., Totsuji, H., and Ichimaru, S. 1977, *Ap. J.*, **218**, 477; erratum 1978, *Ap. J.*, **220**, 742.
 Joss, P. C. 1978, *Ap. J.*, **225**, L123.
 Lamb, D. Q., and Lamb, F. K. 1978, *Ap. J.*, **220**, 291.
 Lewin, W. H. G., and Joss, P. C. 1977, *Nature*, **270**, 211.
 Maraschi, L., and Cavaliere, A. 1978, *Highlights Astr.*, **4**, 127.
 Murakami, T., et al. 1980a, *Ap. J. (Letters)*, **240**, L143.
 ———. 1980b, *Pub. Astr. Soc. Japan*, **32**, 543.
 Sienkiewicz, R. 1980, *Astr. Ap.*, **85**, 295.
 Sugimoto, D., and Fujimoto, M. Y. 1978, *Pub. Astr. Soc. Japan*, **30**, 467.
 Sugimoto, D., and Nomoto, K. 1975, *Pub. Astr. Soc. Japan*, **27**, 197.
 Sugimoto, D., Fujimoto, M. Y., Nariai, K., and Nomoto, K. 1978, in *IAU Symposium 76, Planetary Nebulae Observations and Theory*, ed. Y. Terzian (Dordrecht: Reidel), p. 208.
 ———. 1979, in *IUA Colloquium 53, White Dwarfs and Variable Degenerate Stars*, ed. H. M. Van Horn and V. Weidemann (Rochester: University of Rochester), p. 280.
 Taam, R. E., and Picklum, R. E. 1978, *Ap. J.*, **224**, 210.
 ———. 1979, *Ap. J.*, **233**, 327.
 Tsuruta, S. 1980, in *IAU Symposium 95, Pulsars* (in press).
 Wagoner, R. V., Fowler, W. A., and Hoyle, F. 1967, *Ap. J.*, **148**, 3.
 Woosley, S. E., and Taam, R. E. 1976, *Nature*, **263**, 101.

MASAYUKI Y. FUJIMOTO: Faculty of Education, Niigata University, Niigata 950-21, Japan

TOMOYUKI HANAWA: Department of Astronomy, University of Tokyo, Tokyo 113, Japan

SHIGEKI MIYAJI: Department of Earth Science and Astronomy, College of General Education, University of Tokyo, Meguro-ku, Tokyo 153, Japan